Metal(loid) attenuation processes in an extremely acidic river: the Rio Tinto (SW Spain).

Carlos Ruiz Cánovas [a], Manuel Olías [a] and Jose Miguel Nieto [b]

a) Department of Geodynamics and Palaeontology, University of Huelva (UHU). Facultad de Ciencias Experimentales, Avenida 3 de Marzo s/n, 21071 Huelva, Spain.

b) Department of Geology, University of Huelva (UHU). Facultad de Ciencias Experimentales, Avenida 3 de Marzo s/n, 21071 Huelva, Spain.

Corresponding author: Carlos Ruiz Cánovas (carlos.ruiz@dgeo.uhu.es). Phone: +34 959219870; Fax: +34 959219440

Abstract

This study deals with the hydrogeochemical changes and metal(loid) attenuation processes along the extremely acidic Rio Tinto (SW Spain). The geochemistry of Tinto headwaters is determined by the variability of mining discharges due to different geological, geochemical and hydrological controls. Downstream of the mining area, a decrease in most dissolved element concentrations is recorded. However, not all elements decreased its concentration to the same extent, and even some did not decrease (e.g. Ba and Pb). A group of elements formed by Al, Cd, Co, Cr, Cu, Li, Mg, Mn, Ni and Zn behaved quasi-conservatively; mainly affected by dilution, except at the lower part of the catchment where seem to be affected by sorption/coprecipitation (e.g. Cd, Cu, and Zn) or mineral dissolution processes (e.g. Al, Mg). Iron and As exhibited a non-conservative behaviour due to ochre precipitation and sorption processes, respectively. A group of elements formed by Ca, Na, Sr and Li did not behave conservatively; waters were enriched in these elements by dissolutive reactions of carbonates and aluminosilicates from bedrocks. The behaviour of Pb in the Rio Tinto is complex; values fluctuate along the river course and its solubility may be related to the nature of Fe precipitates.

Keywords: Acid Mine Drainage**,** Principal Component Analysis, Conservative Behaviour, Metal(loid) Removal, Iberian Pyrite Belt.

1. INTRODUCTION

The Rio Tinto (SW Spain) drains materials of the Iberian Pyrite Belt (IPB), a 230 km long by around 50 km wide strip extending from the Seville and Huelva provinces to the southwest of Portugal (Fig. 1). This belt hosts one of the largest concentrations of sulphide deposits in the world (Tornos, 2006) which have been intensely mined for pyrite, base metals and various trace elements since 3000 B.C (Leblanc et al. 2000; Nocete et al. 2005). As a result of this intense mining activity, numerous derelict mines are widespread along the IPB. Among them, the Riotinto Mining District is the most important mining area of the IPB, with a total surface of around 20 km^2 (Cánovas et al. 2007), where the intense mining activity developed during thousands of years has yield a unique landscape with innumerable galleries, waste piles, open pits, tailing dams, etc. The existence of gossans capping orebodies in the IPB indicates that weathering of outcropping sulphide ores could have produced a naturally acidic river system even prior to the beginning of mining (Nocete et al., 2005). The production of acid waters has undoubtedly been increased by the intense mining in the region; however it could be assumed that the natural background concentrations of metals in headwaters were also high in the past, well before any mining occurred (Pérez-López et al 2011).

The long-lasting effects of sulphide oxidation processes in Riotinto has turned the Rio Tinto into a global extreme case of acid mine drainage (AMD) (e.g. López-Archilla and Amils, 1999; Cánovas et al. 2007). Unlike the Odiel River, whose main AMD inputs are widespread along its drainage basin (Sánchez-España et al. 2005; Sarmiento et al. 2009), all AMD discharges join the Rio Tinto in the upper part of its catchment, within the Peña del Hierro and Riotinto mining areas. At its source, the river presents pH values close to 1 and high sulphate (2.4 to 297 g/L) and metal concentrations (Hudson-Edwards et al. 1999; Fernández-Remolar et al. 2005; Hubbard 2007). Downstream, just at its mouth in the Ría of Huelva the Rio Tinto shows a lower level of pollution (Cánovas et al. 2007). Despite the pollutant attenuation observed along its course, the Rio Tinto transports an annually huge metal(loid) load into the Atlantic Ocean, including 15 t of Pb, 12 t of As and 4 t of Cd (Olías et al. 2006). During the tailing pond failure of the Aznalcóllar mine in 1998 almost 14 t of Pb, 3.4 t of Cd and 1.1 t of As were released in the dissolved form (Sainz et al. 2004).

Although the Rio Tinto has been the focus of intense research, there is a lack of information on the hydrochemical changes along its main course. This information is relevant to guess the behaviour and fate of pollutants from AMD sources to the river. Most studies have focused on certain reaches of the river, close to AMD sources (e.g. Ferris et al. 2004; Romero et al. 2006) or just before the confluence with the ocean (e.g. Olías et al. 2006; Cánovas et al. 2007 and 2010; Grande et al. 2011). In this sense, hydrochemical variations along the river course and the neutralization mechanisms of metal(loid) attenuation need to be addressed. This information is still needed to improve the long term knowledge of water quality evolution in AMD affected rivers. Therefore, the main aims of this work are to study the hydrogeochemical evolution and the mechanisms causing metal(loid) attenuation along the Rio Tinto.

2. STUDY AREA

2.1 Geology and mining activity

The Rio Tinto drains materials belonging to the IPB, which corresponds to the South Portuguese Zone of the Hercynian Iberian Massif. Only in the southern part of the catchment the river runs through Neogene materials, mainly marly deposits and biogenic calcarenites (Fig. 1). The IPB comprises three lithological groups belonging to the Upper Palaeozoic: 1) the Phyllite-Quartzite Group (PQ), formed by a sequence of shales and sandstones with an estimated thickness greater than 2000 m (Tornos, 2006), 2) the Volcano-Sedimentary Complex (VSC), which overlies the PQ group and includes a mafic–felsic volcanic sequence interstratified with shales, and 3) the Culm Group, overlying the VSC, in which shales, sandstones and conglomerates prevail. The sulphide mineralization of the IPB are hosted in the VSC as concordant tabular bodies or lenses, commonly underlain by crosscutting stockworks in which sulphides occur in veins and as pervasive disseminations (Sáez et al. 1999). Among them, one of the largest individual polymetallic sulphide deposits in the world is found, the Riotinto orebody, which lies in an east-west anticline, consisting of three distinct mineralized zones: San Dionisio, San Antonio and Cerro Colorado. These orebodies contain pyrite (FeS_2) with minor chalcopyrite ($CuFeS_2$), arsenopyrite (FeAsS), sphalerite (ZnS), galena (PbS) and barite ($BaSO_4$). Detailed geological information of the area can be seen in Nehlig et al. (1998), Saez et al. (1999) and Tornos (2006).

Due to its mineral richness, Riotinto has a long history of mining activities, but only the settlement of advanced civilizations gave rise to intense mining; during the Roman Period around 25 Mt of mineral was extracted in the IPB (Pinedo Vara 1963). The cessation of Roman mining gave rise to a long but discontinuous period of inefficient mining, interrupted with the creation of the Rio Tinto Company, a British consortium which purchased the mine to the Spanish government in 1873. High scale mining was developed in Riotinto from 1873 to 2001 when the mine was derelict. More than 140 Mt of mineral were extracted in the Riotinto mines in this last period (Olías and Nieto 2012), which resulted in a sharp increase in metal pollution in the Riotinto area (van Geen et al. 1997).

2.2 Hydrology

The Rio Tinto has its source in the vicinity of the Peña Del Hierro mining complex as a result of the confluence of several drainages emerging from wastes piles. Downstream, the Rio Tinto crosses the Riotinto mining complex, where receives an innumerable number of acidic discharges from underground galleries, spoil heaps, settling ponds, tailing dams, etc. The main tributaries that are not affected by AMD join the river downstream of the mining area. The main tributaries of the Rio Tinto are the Jarrama Creek and the Corumbel River on its left bank, which have been regulated by reservoirs, and the Candón Creek on its right bank (Fig. 1). As the slope decreases, the river broadens; losing its fluvial character in the surroundings of San Juan del Puerto (Fig. 1), and joining the Odiel River in a common estuary known as Ria of Huelva.

The climate is of a dry Mediterranean type with an average rainfall varying between 600 mm in the lower part of the catchment and 1000 mm in the upper northern hills. The rainfall distribution displays great inter- and intra-annual variations, with 70% of the annual rainfall occurring between October and February, while rainfall is almost non-existent during the dry season from June to September (Olías et al. 2011). The Tinto basin is composed mainly by impermeable materials; therefore the river has a low natural regulation, and most of the water discharge occurs during flood events.

3 METHODOLOGY

Four different in-situ sampling campaigns were performed along the main course of the Rio Tinto from June 2005 to June 2006. Five different sampling points were selected (Samples TR; Fig. 1 left)

120 in order to study the spatial hydrogeochemical variations of the Rio Tinto. Additionally, samples
121 from headwaters and main AMD inputs were collected in the mining area (Samples T; Fig. 1 right)
122 during the last sampling in June 2006. Flow river data were obtained from point TR4 (Fig. 1), the
123 unique working stream-gauging station within the catchment. The study period was some drier than
124 normal; the average precipitation in the watershed was below 600 mm yr^{-1}. Two samplings took
125 place during the dry period (Fig. 2) characterized by extremely low river flows (14 and 30 L/s in
126 June 2005 and 2006; Fig. 2). Two samplings were also performed during the rainy period (November
127 2005 and February 2006) although did not coincide with flood events. The river flow during both
128 samplings was below 1 m^3/s (0.2 and 0.5 m^3/s, respectively; Fig. 2) despite the rainfalls collected
129 during the preceding month (67 and 95 mm, respectively). Releases from freshwaters reservoirs had
130 little influence on the river during the surveys (Fig. 2).
131
132 Samples were taken at 1 m from the riverbank to avoid problems associated to water stagnation.
133 Then, they were filtrated with Millipore Teflon filters of 0.45 μm, which implies that some colloidal
134 particles with lower diameter are considered as dissolved (Langmuir 1997). Collected samples were
135 preserved in pre-washed polyethylene containers and acidified with HNO_3 suprapur Merk® to pH<
136 2. Finally, samples were kept at dark in the refrigerator (around 4ºC). Temperature, electrical
137 conductivity (EC), pH and redox potential (Eh) were determined in the field with portable meters
138 (Hanna Instruments HI-9025 and HI-9033). The measurement errors for these instruments were
139 from 0.1 to 0.001 mS/cm (around 1% of the measurement range), 0.2ºC, 0.02 and 2 mV,
140 respectively. The instruments were calibrated against certified standards before carrying out the
141 samplings. To measure Eh, a probe with a platinum electrode and an Ag/AgCl reference electrode
142 was used. The values of Eh were corrected in order to obtain the potential referred to the hydrogen
143 electrode (Nordstrom and Wilde 1998).
144
145 Analyses were performed in the Central Research Services of the University of Huelva, using
146 Inductively Coupled Plasma Optical Emission Spectroscopy (ICP-OES) on a Jobin Yvon (JY
147 ULTIMA 2) spectrometer equipped with a cyclonic concentric nebulizer in order to decrease the
148 detection limit of the equipment. The method used (Ruiz et al. 2003) was especially designed to
149 estimate major, minor and trace elements in waters affected by AMD. Different elements such as
150 Al, As, Ba, Be, Ca, Cd, Co, Cr, Cu, Fe, K, Li, Mg, Mn, Na, Ni, Pb, S, Si, Sn, Sr, and Zn were

151 analyzed. Samples out of range were diluted at a maximum dilution factor of 1:20 with Milli-Q
152 water (18.2 MΩ·cm); HNO3 suprapur Merk® was added to maintain the pH below 2. The quality
153 of analysis has been verified with a NIST-1640 certified reference material. A triplicate analysis was
154 performed in order to evaluate the precision, being better than 5% in all cases. In each analysis
155 sequence, standards were also used to check the accuracy. Blanks were also analyzed, being all
156 elements below the detection limit of the equipment. Additionally, the PHREEQC code (Parkhurst
157 and Appelo 1999) with the WATEQ4F database was used to calculate solution charge balance as a
158 Quality Assurance and Quality Control (QA/QC) measure for solution compositions. An 88% of
159 samples collected (24 out of 27) were stochiometrically balanced within ±5% of error.
160
161 The PHREEQC code v2.17.01 (Parkhurst and Appelo 1999) was employed to study the chemical
162 speciation and saturation indices using the Wateq4f database, enlarged with thermodynamic data
163 from Bigham et al. (1996) for the solubility of schwertmannite and ferrihydrite. A Principal
164 Component Analysis (PCA) has been performed on data from chemical analysis to infer patterns of
165 behaviour in selected variables. The use of PCA allows the number of variables in a multivariate
166 data set to be reduced, whilst retaining as much as possible of the variation present in the data set.
167 The Spearman's correlation matrix has been used for the PCA due to some variables do not show a
168 normal distribution (Davis 1986). All variables were standardized to z-scores. Missing data (n< 2)
169 in some elements (As, Ca, Cr, Cu, Li, Sr and Na; Table 2) were replaced by the nearest neighbours
170 value. Barium, Be and K were not included due to the high missing values (n> 5) observed for these
171 elements.
172
173
174 **4 RESULTS**
175
176 **4.1 Sources of AMD**
177 The Rio Tinto has its source at several drainages from spoil heaps in the Peña de Hierro Mine
178 (sampling point T1; Fig. 1), with low pH and high EC values (2.06 and 21.9 mS/cm, respectively;
179 Table 1). As a result of intense sulphide oxidation processes high concentrations of sulphate and Fe
180 are found (41 and 10 g/L, respectively; Table 1) yielding a Fe/SO_4 mass ratio of 0.25, close to the
181 theoretical value indicative of oxidative pyrite dissolution (0.29). The metal(loid) concentration of

182 Tinto headwaters is controlled by the mineralogy of the spoil heaps (mainly pyrite and other
183 accessories sulphides from mineralization, as well as micas quartz, etc. from host rocks and hematite
184 from toasted pyrite; e.g. Romero et al. 2006) from which it is originated, showing a low content in
185 Cu and Zn (10 and 15 mg/L) but high concentrations of Mn, As, Co or Pb (Table 1). The dissolution
186 of the surrounding host rocks (e.g. volcanic rocks, slates) by AMD explains the high concentrations
187 of Al, Mg, Ca, Li or Sr (Table 1).
188
189 Downstream of its source, several drainages from others spoils join the river modifying its pH,
190 colour and metal(loid) content (sample T2; Table 1). Before the Marismilla Reservoir (Fig. 1), the
191 Rio Tinto crosses an extensive area of sulphide-rich wastes where several diffuse AMD inputs
192 increase sulphate and metal concentrations (e.g. 17 g/L of sulphate, 2.1 g/L of Fe, 379 mg/L of Cu;
193 sample T3, table 1). Downstream of this dam, at around 4.5 km from its source, the river receives
194 one of its main metal(loid) input, the Tunnel 11 discharge, which drains the underground workings
195 of Filón Sur. This drainage has pH values between 2.4 and 2.7, and high sulphate and metal
196 concentrations (e.g. 10-18 g/L of sulphate, 1.1-2.1 g/L of Fe, 249-463 mg/L of Cu; Hubbard 2007).
197 At around 7 km from its source, the river receives the acidic discharges from Tunnel 16, which
198 drains the underground workings of San Dionisio (Pozo Alfredo and Corta Atalaya; Fig. 1) before
199 mixing with discharges coming from two large settling ponds (Hubbard 2007). The combination of
200 these discharges has a moderate content of metal and sulphates (e.g. 3.7 g/L of sulphate, 735 mg/L
201 of Fe, 90 mg/L of Zn, 47 mg/L of Cu; sample T6, Table 1) due to mixing with discharge from two
202 large settling ponds. However, Tunnel 16 hydrochemistry seems to have changed along the time
203 (Hubbard 2007) related to the lack of pumping labours in Pozo Alfredo, and as a consequence the
204 flooding of Corta Atalaya pit has been accelerated in recent years.
205
206 Downstream, the river receives the acidic discharges from the Zarandas-Naya zone, a derelict
207 processing complex where the ore was crushed, piled and leached to obtain Cu (Hubbard 2007). The
208 largest discharge in volume of Zarandas-Naya is the Alcojola Creek which shows high acidity and
209 a huge concentration of sulphate and metal(loid)s (pH 1.6, 32 g/L of sulphate, 12 g/L of Fe, 41 mg/L
210 of As, 2 mg/L of Pb; Table 1). As a result of the confluence of Alcojola Creek, the Rio Tinto
211 increases its acidity, mineralization (7.4-9.0 mS/cm), sulphate and metal(loid) content. This

212 contradicts the extremely low EC values (interquartil range of 12-14 μS/cm) reported by De la Torre
213 et al. (2011) which may be mistaken.
214
215 **4.2 Downstream of the mining area**
216
217 Downstream of Zarandas, the Rio Tinto does not receive any other AMD input. The metal(loid)
218 contribution from the tributaries is negligible. The results obtained during the sampling campaigns
219 (June and November 2005 and February and June 2006) along the river course are shown in Table
220 2 and Figure 3. A spatial pattern in pH-Eh conditions can be observed; higher pH and Eh values are
221 found downstream. At the same time, EC values and most element concentrations decrease, except
222 for Ba (not shown in Fig. 3).
223
224 A useful tool for identifying the mechanisms responsible for metal(loid) removal in water courses
225 is the comparison to a conservative component. Sulphate is recommended as the best conservative
226 component in AMD polluted waters, as it is not affected by the fluctuation of pH (Bencala et al.
227 1987; Gray 1998). Although sulphate in AMD can be removed from solution by sorption or
228 precipitation reactions (e.g. Nordstrom 1982; Bigham et al. 1990) if its concentration is significantly
229 high compared to Fe and Al, it can be considered as conservative (Berger et al. 2000).
230
231 As the sulphate contribution downstream of the mining area is almost negligible, normalizing the
232 metal(loid)/sulphate (Me/SO_4) mass ratios in relation to TR2 (Fig. 1) we can infer the behaviour of
233 different metal(loid)s along the Tinto river course. Thus, normalized values of
234 $(Me/SO_4)/(Me/SO_4)_{TR2}$ above 1 would indicate metal(loid) addition into solution through mineral
235 dissolution or desorption from mineral surfaces, whereas values below 1 would involve metal(loid)
236 removal through mineral precipitation or sorption. Normalized values close to 1 would indicate a
237 quasi-conservative behaviour.
238
239 The concentration of Fe and, especially, As decreases sharply in relation to sulphate (Fig. 4). This
240 decreasing ratio implies the removal of both elements downstream of the mining area, being more
241 intense in the southern reaches of the river (TR4 and TR5). Some elements such as Al, Mn, Mg and
242 Ni seem to have a quasi-conservative behaviour as show values close to 1 (Fig. 4), suggesting

243 dilution as the only responsible for the decrease in concentration observed downstream of the mining
244 area (Table 2 and Fig. 3). Chromium also appears to have a quasi-conservative behaviour; only an
245 increase of the normalized Cr/SO_4 mass ratio was observed between TR2 (the mining area) and TR3
246 (Fig. 4) in November 2006, remaining almost constant downstream. Other elements such as Cu, Zn,
247 Cd and Co also behave quasi-conservatively in the upper reaches of the river, meanwhile
248 downstream decreased its concentration in respect with sulphate. On the other hand, a strong
249 enrichment in Ca, Si, Na, Sr and Pb is observed downstream of the mining area (Fig. 4). This
250 enrichment is notably evident for Ca, Si, Na and Sr between TR4 and TR5.
251
252 A Principal Component Analysis (PCA) of the results has been carried out to identify relationships
253 between variables and behaviour patterns of elements from TR2 (the end of the mining zone) to
254 TR5. The first component describes a 79% of variance and it is related to water mineralization (Fig.
255 5A). Most variables (Al, Cd, Cu, Fe, Mn, etc.) are placed on the positive side of component 1(Fig.
256 5B) while pH is on the negative as acidity enhances metal solubility. The second component
257 describes only an 8.6% of variance and most variables (Cd, Al, Co, Cu, Cr, Li, Mg, Mn, Ni, sulphate
258 and Zn) show values close to 0. In turn, it can be seen a group of elements located either on the
259 positive side together Eh (i.e. Pb, Ca, Sr, Na and Si) or on the negative (i.e. Fe and As; Fig. 5A).
260 This component seems to be related to certain geochemical reactions (i.e. ochre precipitation,
261 sorption and bedrock mineral dissolution) that will be approached later.
262
263 The PCA performed on samples also evidences seasonal and spatial differences on the Rio Tinto
264 hydrochemistry. Samples collected within the mining area (TR2) are placed on the positive side of
265 component 1 and on the negative of component 2 due to the high metal(loid) concentrations
266 (especially for As and Fe). These samples represent the AMD sources (an exception is the sample
267 collected in June 2005 which showed lower values of Fe and As than the rest; Fig. 5C). Samples
268 collected downstream (TR3 to TR5) move progressively towards the negative side of component 1,
269 due to the decrease in element concentrations and the increase of pH/Eh values. On the other hand,
270 it can be noted a progressive displacement of samples towards the positive side of component 2 (Fig.
271 5C) owing to the decrease in Fe and As concentrations and the increase in Ca, Si, Na, Sr, Pb and Eh
272 values. The enrichment in Ca, Si, Sr and Na is especially significant during the dry season; it can be

noted the displacement of samples toward the positive side of component 2 (Figure 5D) where these elements are located.

5. DISCUSSION

5.1 Dilution

As shown in Figure 4 the main process controlling downstream evolution of the dissolved concentrations of most elements in the Rio Tinto is dilution (according to the PCA, dilution would explain 79% of the variance). This effect is evidently more significant during the rainy period; on the other hand, dilution processes were less intense in June 2005 than in 2006. The concentration of Al, Co, Cr, Li, Mg, Mn and Ni, once released to Rio Tinto, depends only on dilution. The concentration of Cd, Cu and Zn is also controlled by dilution, although they also appear to be affected by coprecipitation in the lower reaches of the river.

5.2 Fe precipitation

Besides the acidity released from the different AMD discharges, the main processes which affect the H^+ balance in the Rio Tinto are: a) Fe(II) oxidation catalyzed by chemolithotrophic bacteria (Eq. 1) and b) Fe(III) ochre precipitation (simplified example in Eq. 2). Both processes influence pH by removal and release of H^+ into water, respectively. According to the results obtained by the speciation calculation with PHREEQC, Fe is mainly found as Fe(II) in the mining area (from 72 to 95% of total Fe) with higher values during the rainy period.

$$Fe^{2+} + \tfrac{1}{4} O_2 + H^+ \longrightarrow Fe^{3+} + \tfrac{1}{2} H_2O \qquad \text{Eq. 1}$$

$$Fe^{3+} + 3\,H_2O \longrightarrow Fe(OH)_3^{3+} + 3H^+ \qquad \text{Eq. 2}$$

Downstream of Zarandas, once the river leaves the mining area, the input of iron-rich lixiviates ceases. Therefore, the concentration of Fe(II) decreases progressively (from 1 to 43% of total Fe) by oxidation. The intensity of these processes is higher during summer when bacterial catalysis

speeds up oxidation reactions due to high temperatures. As long as Fe(II) is oxidized, Fe(III) ochre precipitation becomes the dominant process in the H^+ balance. The release of H^+ by this reaction buffers pH despite the dilution effect exerted by downstream tributaries; values remain below 3 along the entire river course (Fig. 3). However, during floods pH can reach values close to 5 (Cánovas et al 2012).

A change in Eh values takes place downstream of the mining area (Fig. 3), reaching more oxidant conditions due to Fe(II) oxidation processes and favouring Fe precipitation, as in others AMD-affected environments (Nordstrom and Alpers 1999). Figure 6 shows the water saturation indices (SI) respect to some of the most common precipitating Fe minerals in AMD systems. All water samples were undersaturated in amorphous $Fe(OH)_3$ due to the low pH (below 3) of the solution. However, waters showed oversaturation respect to K-jarosite and plumbojarosite along the river course. During the dry period, other jarositic minerals such as Na-jarosite and H-jarosite could exert a control on Fe solubility as SI values come over 0 (Fig. 6). In the lower part of the catchment (at higher pH values and lower Fe and sulphate concentrations), the SI values for schwertmannite are close to 0 (Fig. 6), which suggests the possible precipitation of this mineral. Figure 7 represents the activity of Fe^{3+} vs pH for all collected samples. Most samples fall in the stability window for jarosite and only some belonging to the lowest reaches of the river (TR3, TR4 and TR5) are found close to the stability window for schwertmannite. This supports jarosite as the main mineral phase controlling Fe solubility in Tinto waters. Some authors (Hudson-Edwards et al. 1999; Galan et al. 2003) found jarosite in the sediments of the Rio Tinto.

Figure 8A shows the Fe/SO_4 mass ratio evolution along the Rio Tinto. It can be noted the lower values of Fe/SO_4 mass ratio observed at points further downstream as a consequence of Fe ochre precipitation. The amount of Fe removed from solution along the Rio Tinto can be estimated from the dilution factor calculated taking sulphate as a conservative component, as shows Equation 3:

$$C_r(\%) = \left[\left(C_{cal} - C_{meas}\right) / C_{cal}\right] \times 100 \qquad \text{Eq. 3}$$

where C_r is the amount of Fe precipitated from solution, C_{meas} is the concentration measured at each point and C_{cal} is the concentration calculated by dilution factors (obtained as sulphate concentration

329 at each point divided by sulphate concentration at TR2). Thus, estimations provide a Fe removal rate
330 of around 50% and 70% at the lowest reach of the river (TR5) during the dry and rainy seasons,
331 respectively.
332
333 **5.3 Coprecipitation processes**
334
335 The newly formed Fe precipitates have low cristallinity, very small particle size and high specific
336 surface area, becoming very efficient sorbents of metals (Dzombak and Morel 1990, Smith 1999).
337 Figures 8B to D show the relationship between the Fe/SO_4 mass ratio and the concentration of As,
338 Cr and Pb, respectively. These relationships have been previously used in the adjacent Odiel River
339 (Olias et al. 2004) as a tool to identify metal(loid) incorporation in ochre precipitates. It can be
340 established a good correlation between Fe/SO_4 mass ratio and As concentrations in Tinto waters,
341 which supports the incorporation in Fe precipitates as the main control of As concentration along
342 the river course. Also the location of As near Fe in the PCA is just consistent with this interpretation.
343 This finding is also supported by other studies in the area (e.g. Olias et al. 2004; Asta et al. 2010;
344 Pérez-López et al. 2011) and in other AMD settings (e.g Regenspurg and Peiffer 2005).
345
346 The removal of As (and Fe) is more intense in the lower reach of the river where the water residence
347 time is higher as a consequence of the river broadening. The apparent conservative behaviour
348 exhibited by As in June and November 2005 (TR3) and in June 2005 (TR4), where the normalized
349 mass ratio even increases, must be related to the scarce removal of Fe at this point, as suggests the
350 normalized Fe/SO_4 ratio (Fig. 4).
351
352 The decreasing concentrations of Cu, Zn, Cd and Co in the lower part of the river may be influenced
353 by sorption processes onto Fe mineral phases which are especially significant in June 2006 (Fig. 4).
354 Although it has been widely reported the tendency of other elements such as Cr and Pb to be sorbed
355 onto Fe precipitates in AMD environments (e.g. Accornero et al. 2005; Regenspurg and Peiffer
356 2005) it seems these processes are less influential for both elements in this study. Figure 8C shows
357 a poor correlation between Fe/SO_4 and Cr concentration. The quasi-conservative behaviour of Cr
358 and the scarce influence of these processes on its concentration were previously pointed by the PCA
359 and the Cr/SO_4 ratio evolution (Fig. 4).

5.4 Other processes

The enrichment in Ca, Si, Sr and Na observed in Figure 4 is caused by the dissolution of carbonates and aluminosilicates, which is especially significant in the lower part of the catchment and during the dry season.

On the other hand, the high concentration of sulphate in Tinto waters can affect the solubility of some minerals. This is the case for Ba which concentration is strongly controlled by barite in the Rio Tinto (e.g. Cánovas et al. 2007). On the contrary, gypsum, epsomite and celestite were undersaturated in all surveys, and therefore a solubility control by these minerals for Ca, Mg and Sr is not expected. In the case of Pb, this control is still not clear. No correlation could be established between Fe/SO_4 and Pb concentration (Fig. 8D) and the ratio Pb/SO_4 increases clearly downstream. In this sense, concentration of Pb seems to be controlled by the nature of Fe precipitates; schwertmannite precipitation is less effective retaining Pb than jarosite (Acero et al. 2006; Cánovas et al. 2010). This could explain the higher Pb concentrations observed in the lower reach of the river, where SI values for schwertmannite are close to 0. On the other hand, its solubility can be also affected by anglesite precipitation; the decrease of sulphate concentration downstream could contribute to the high concentrations of Pb in this zone.

CONCLUSIONS

The Rio Tinto is deeply contaminated by acid mine drainage (AMD) due to the vast number of acidic discharges received from the Peña del Hierro and Riotinto mining complexes, located in the upper part of the catchment. The geochemistry of Tinto headwaters is determined by the variability of mining discharges due to a variety of geological, geochemical and hydrological controls. The pH in the Tinto headwaters fluctuates as a consequence of the arrival of ferrous and ferric lixiviates, and the simultaneous occurrence of Fe(II) oxidation and Fe(III) ochre precipitation processes. Once the input of ferrous waters ceases as the Rio Tinto leaves the mining area, Fe(III) ochre precipitation becomes the dominant process, buffering pH (below 3) along the entire river course despite the dilution effect of freshwaters.

Downstream of the mining area, a general decrease in water mineralization and in most element concentrations (e.g. Al, Fe, Cu, Zn, As, Cd, Co and sulphate) is observed. Iron and As exhibited a non-conservative behaviour; they are affected by ochre precipitation and sorption processes. Although the term "ochre" in AMD environments refers to a mixture of metastable Fe mineral phases, jarosite seems to be the most probable Fe precipitating mineral along the Rio Tinto.

The different behaviour followed by elements is dictated by geochemical controls such as mineral dissolution/precipitation reactions, sorption processes, etc. In this way, a group of elements formed by Al, Cd, Co, Cr, Cu, Li, Mg, Mn, Ni and Zn, seems to be mainly affected by dilution. However, at the lower part of the catchment these elements may be affected by sorption/coprecipitation (i.e. Cd, Cu, and Zn) or mineral dissolution processes (i.e. Al, Mg). On the other hand, a group of elements formed by Ca, Na, Sr and Li is affected by dissolutive reactions of carbonates and aluminosilicates from bedrocks, especially intense in the lower part of the catchment and during the dry season. The behaviour of Pb in the Rio Tinto is complex; its concentration along the river course is maintained and its solubility seems to be related to the nature of Fe precipitates (i.e. schwertmannite, jarosite, and anglesite).

A clear seasonal pattern can be identified downstream; during the rainy period the diluting effect of freshwaters is the more influential factor in the Rio Tinto hydrochemistry, while during the dry period the dissolution of minerals from bedrocks (carbonate and aluminosilicates), the ochre precipitation and sorption of metal(loid)s gain importance in the Rio Tinto hydrochemistry.

ACKNOWLEDGEMENTS

This work has been financed by the Spanish Ministry of Education and Science through project CGL2010-21956-C02. The authors wish to thank the Environmental Council of the Andalusian Regional Government for the information provided for this study. The comments and helpful criticisms of two anonymous reviewers and the support of the Editor-in-chief Dr. Jack T. Trevors have considerably improved the original manuscript and therefore are also gratefully acknowledged.

420 **REFERENCES**

421 Accornero M., Marini L., Ottonello G., & Vetuschi Zuccolini M. (2005). The fate of major
422 constituents and chromium and other trace elements when acid waters from the derelict
423 Libiola mine (Italy) are mixed with stream waters. Applied Geochemistry 20, 1368-1390.

424 Acero P., Ayora C., Torrento C., & Nieto J.M. (2006). The behavior of trace elements during
425 schwertmannite precipitation and subsequent transformation into goethite and jarosite.
426 Geochimica et Cosmochimica Acta 70, 4130-4139.

427 Asta, M.P., Ayora, C., Román-Ross, G., Cama, J., Acero, P., Gault, A.G., Charnock, J.M., &
428 Bardelli, F. (2010). Natural attenuation of arsenic in the Tinto Santa Rosa acid stream (Iberian
429 Pyritic Belt, SW Spain): The role of iron precipitates. Chemical Geology 271, 1-12.

430 Bencala, K.E., McKnight D.M., & Zellweger G.W. (1987). Evaluation of natural tracers in an
431 acidic and metal-rich stream. Water Resources Research 23, 827-836.

432 Berger A.C., Bethke C.M., & Krumhansl M.L. (2000). A process model of natural attenuation in
433 drainage from a historic mining district. Applied Geochemistry 15, 655-666.

434 Bigham J.M., Schwertmann U., Carlson L., & Murad E. (1990). A poorly crystallized
435 oxyhydroxysulfate of iron formed by bacterial oxidation of Fe(II) in acid mine waters.
436 Geochimica et Cosmochimica Acta 54, 2743-58.

437 Bigham J.M., Schwertmann U., Traina S.J., Winland R.L., & Wolf M. (1996). Schwertmannite
438 and the chemical modeling of iron in acid sulfate waters. Geochimica et Cosmochimica Acta
439 60(12), 2111-2121.

440 Cánovas C.R., Olias M., Nieto J.M., Sarmiento A.M., & Cerón J.C. (2007). Hydrogeochemical
441 characteristics of the Odiel and Tinto rivers (SW Spain). Factors controlling metal contents.
442 Science of the Total Environment 373, 363-382.

443 Cánovas C.R., Hubbard C.G., Olías M., Nieto J.M., Black S., & Coleman M.L. (2008).
444 Hydrochemical variations and contaminant load in the Río Tinto (Spain) during flood events.
445 Journal of Hydrology 350 (1-2), 24-40.

446 Cánovas C.R., Olías M., Nieto J.M., & Galván L. (2010). Wash-out processes of evaporitic sulfate
447 salts in the Tinto river: Hydrogeochemical evolution and environmental impact. Applied
448 Geochemistry 25 (2), 288-301.

449 Cánovas C.R., Olías M., Vázquez-Suñé E., Ayora C., & Nieto J.M. (2012). Influence of releases
450 from a fresh water reservoir on the hydrochemistry of the Tinto River (SW Spain). Science
451 of the Total Environment 416, 418-428.

452 Davis J.C. (1986). Statistics and data analysis in geology. Singapore: John Wiley & Sons. 646 p.

453 De la Torre M.L., Grande J.A., Graiño J., Gómez T., & Cerón J.C. (2011). Characterization of
454 AMD Pollution in the River Tinto (SW Spain). Geochemical Comparison between
455 Generating Source and Receiving Environment. Water Air and Soil Pollution 216(3), 3-19.

456 Dzombak D.A., & Morel F.M. (1990). Surface Complexation Modelling: Hydrous Ferric Oxide.
457 John Wiley, New York.

458 Fernández-Remolar D.C., Morris R.V., Gruener J.E., Amils R., & Knoll A.H. (2005). The Río
459 Tinto Basin, Spain: Mineralogy, sedimentary geobiology, and implications for interpretation
460 of outcrop rocks at Meridiani Planum, Mars. Earth Planetary Science Letters 240, 149-167.

461 Ferris F.G., Hallbeck L., Kennedy C.B., & Pedersen K. (2004). Geochemistry of acidic Rio Tinto
462 headwaters and role of bacteria in solid phase metal partitioning. Chemical Geology 212,
463 291-300.

464 Galán E., Gómez-Ariza J.L., González I., Fernández-Caliani J.C., Morales E., & Giráldez, I.
465 (2003). Heavy metal partitioning in river sediments severely polluted by acid mine drainage
466 in the Iberian Pyrite Belt. Applied Geochemistry.18, 409-421.

467 Grande J.A., Aroba J., Andújar J.M., Gómez T., De la Torre M.L., Borrego J., Romero S., Barranco
468 C., & Santisteban M. (2011). Tinto Versus Odiel: Two AMD polluted rivers and an
469 unresolved issue. An Artificial Intelligence Approach. Water Resource Management 25(15),
470 3575-3594.

471 Gray N.F. (1998). Acid mine drainage composition and the implications for its impact on lotic
472 systems. Water Research 32, 2122–2134.

473 Hubbard C.G. (2007). Acid mine drainage generation and transport processes in the Tinto River,
474 SW Spain. PhD Thesis. University of Reading (UK).

475 Hudson-Edwards K.A., Schell C., & Macklin M.G. (1999). Mineralogy and geochemistry of
476 alluvium contaminated by metal mining in the Rio Tinto area, southwest Spain. Applied
477 Geochemistry 14, 1015-1030.

478 Langmuir D. (1997). Aqueous environmental geochemistry. Prentice Hall, Upper Saddle River

479 Leblanc M., Morales J.A., Borrego J., & Elbaz-Poulichet F. (2000). 4,500-Year-old mining
480 pollution in southwestern Spain: Long-term implications for modern mining pollution.
481 Economic Geology 95, 655-661.

482 López-Archilla A.I., & Amils R. (1999). A Comparative Ecological Study of Two Acidic Rivers
483 in Southwestern Spain. Microbial Ecology 38(2), 146-156.

484 Nehlig P., Cassard D., & Marcoux E. (1998). Geometry and genesis of feeder zones of massive
485 sulphide deposits: constraints from the Rio Tinto ore deposit (Spain). Mineralium Deposita
486 33, 137-149.

487 Nocete F., Alex E., Nieto J.M., Sáez R., & Bayona M.R (2005). An archaelogical approach to
488 regional environmental pollution in the south-western Iberian Peninsula related to Third
489 Millenium B.C mining and metallurgy. Journal of Archaeological Science 32(10), 1566-
490 1576.

491 Nordstrom D.K. (1982). The effect of sulfate on aluminum concentrations in natural waters: some
492 stability relations in the system Al_2O_3-SO_3-H_2O at 298 K. Geochimica et Cosmochimica Acta
493 46(4), 681-692.

494 Nordstrom D.K., & Wilde F.D. (1998). Reduction–oxidation potential (electrode method). In:
495 National field manual for the collection of water quality data, U.S. Geological Survey
496 techniques of water-resources investigations, book 9; chapter 6.5.

497 Nordstrom D.K., & Alpers C.N., (1999). Geochemistry of acid mine waters Chapter 6. In: Plumlee,
498 G.S., Logsdon, M.J. (Eds.), The Environmental Geochemistry of Mineral Deposits, 1999.
499 Rev. Econ. Geol., Vol. 6A. Soc. Econ. Geol. Inc, Littleton, Colorado, pp. 133–160.

500 Olías M., Nieto J.M., Sarmiento A.M., Cerón J.C., & Canovas C.R. (2004). Seasonal water quality
501 variations in a river affected by acid mine drainage: The Odiel river (south west Spain).
502 Science of the Total Environment 333, 267-281.

503 Olías M., Cánovas C.R., Nieto J.M., & Sarmiento A.M. (2006). Evaluation of the dissolved
504 contaminant load transported by the Tinto and Odiel rivers (South West Spain). Applied
505 Geochemistry 21, 1733-1749.

506 Olías M., Nieto J.M., Sarmiento A.M., Cánovas C.R., & Galván L. (2011). Water quality in the
507 future Alcolea Reservoir (Odiel River, SW Spain): a clear example of inappropriate
508 management of water resources in Spain. Water Resources Management 25, 201-215.

509 Olías M., & Nieto J.M. (2012). El impacto de la minería en los ríos Tinto y Odiel a lo largo de la
510 historia. Revista de la Sociedad Geológica de España, 25(3-4), 177-192

511 Parkhurst D.L., & Appelo C.A.J. (1999). User's guide to PHREEQC (Version 2). A computer
512 program for speciation, batch reaction, one-dimensional transport, and inverse geochemical
513 calculations. USGS water-resources investigations report 99-4259. Denver, Colorado.

514 Pérez-López R., Asta M.P., Román-Ross G., Nieto J.M., Ayora C., & Tucoulou R. (2011).
515 Synchrotron-based X-ray study of iron oxide transformations in terraces from the Tinto-Odiel
516 river system: Influence on arsenic mobility. Chemical Geology 280, 336–343.

517 Pinedo Vara I. (1963). Piritas de Huelva. Su historia, minería y aprovechamiento. Ed. Summa,
518 Madrid.

519 Regenspurg S., & Pfeiffer S. (2005). Arsenate and chromate incorporation in schwertmannite.
520 Applied Geochemistry 20, 1226–1239.

521 Romero A., González I., & Galan E. (2006). The role of efflorescent sulfate salts in the storage of
522 trace elements in stream waters polluted by Acid Mine Drainage: The case of Peña del Hierro,
523 southwestern Spain. Canadian Mineralogist 44, 1431-1446.

524 Ruiz, M.J., Carrasco, R., Perez, R., Sarmiento, A.M., & Nieto, J.M. (2003). Optimizacion del
525 analisis de elementos mayores y traza mediante UN-ICP-OES en muestras de drenaje acido
526 de mina. Proceedings of the IV Iberian Geochemical Meeting, 14–18 Julio, Coimbra,
527 Portugal, Universidad de Coimbra, pp. 402–404.

528 Sáez R., Pascual E., Toscano M., & Álmodóvar G.R. (1999). The Iberian type of volcano-
529 sedimentary massive sulphide deposits. Mineralium Deposita 34, 549-570.

530 Sainz A., Grande J.A., & de la Torre M.L. (2004). Characterisation of heavy metal discharge into
531 the Ria of Huelva. Environment International 30, 557-566.

532 Sanchez España J., Lopez Pamo E., Santofimia E., Aduvire O., Reyes J., & Barettino D. (2005).
533 Acid mine drainage in the Iberian Pyrite Belt (Odiel river watershed, Huelva, SW Spain):
534 Geochemistry, mineralogy and environmental implications. Applied Geochemistry 20, 1320-
535 1356.

536 Sarmiento A.M., Olías M., Nieto J.M., Cánovas C.R., & Delgado J. (2009). Natural attenuation
537 processes in two water reservoirs receiving acid mine drainage. Science of the Total
538 Environment 407, 2051-2062.

539 Smith K.S. (1999). Metal sorption on mineral surfaces: an overview with examples relating to
540 mineral deposits. In: The Environmental Geochemistry of Mineral Deposits. Reviews in
541 Economic Geology, Vol. 6A, Ed. Plumlee, G. S. and Logsdon, M. J., 161-182.

542 Tornos F. (2006). Environment of formation and styles of volcanogenic massive sulfides: The
543 Iberian Pyrite Belt. Ore Geology Reviews 28 (3), 259-307.

van Geen A., Adkins J.F., Boyle E.A., Nelson C.H., & Palanques A. (1997). A 120-yr record of widespread contamination from mining of the Iberian pyrite belt. Geology 25(4), 291-294.

FIGURE CAPTIONS

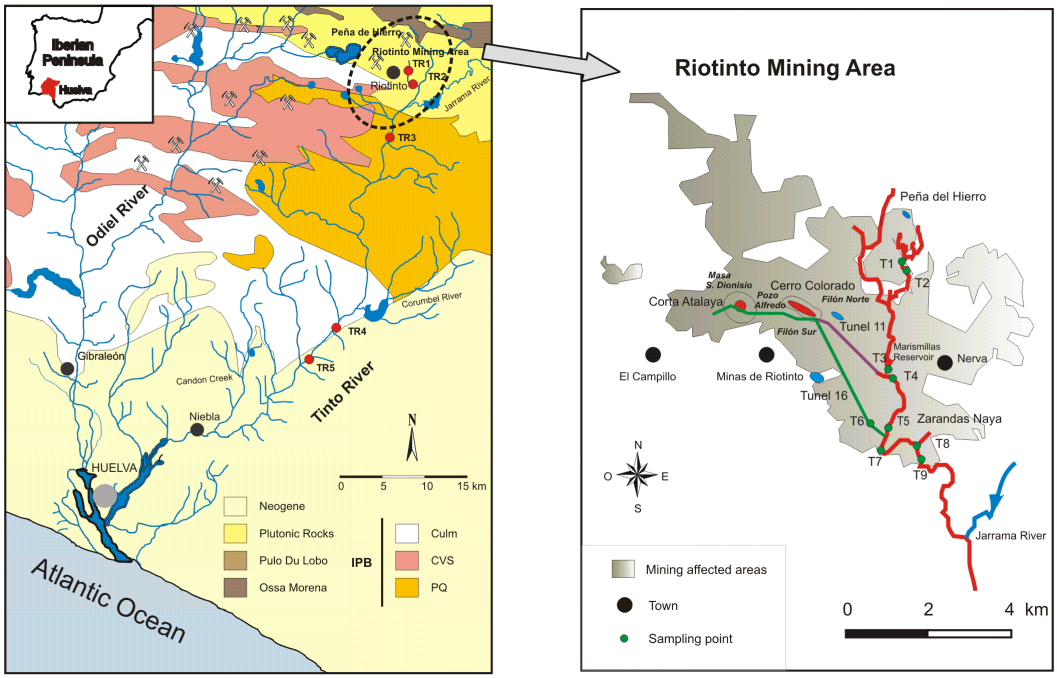

Figure 1. A) Geological map of the Rio Tinto basin, indicating the main sampling points along its course. B) Detailed map of the Riotinto Mining District (modified from Hubbard, 2007), showing the different samples collected in June 2006.

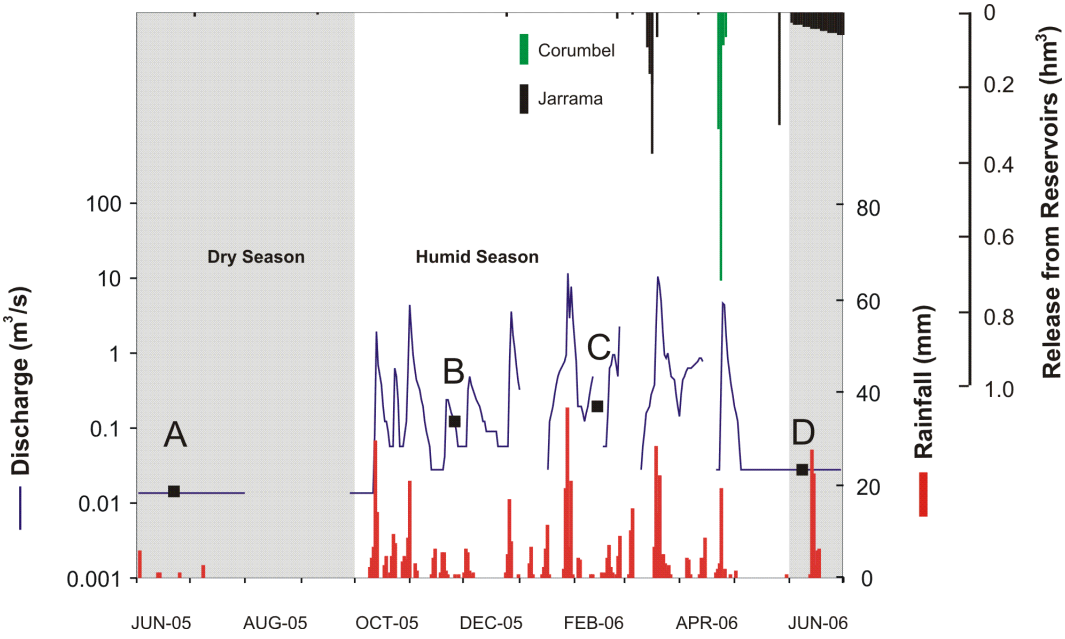

Figure 2. Hydrograph of the Rio Tinto during the study period, indicating the average rainfall recorded in the basin, releases from Corumbel and Jarrama reservoirs and the occurrence of samplings (A-D).

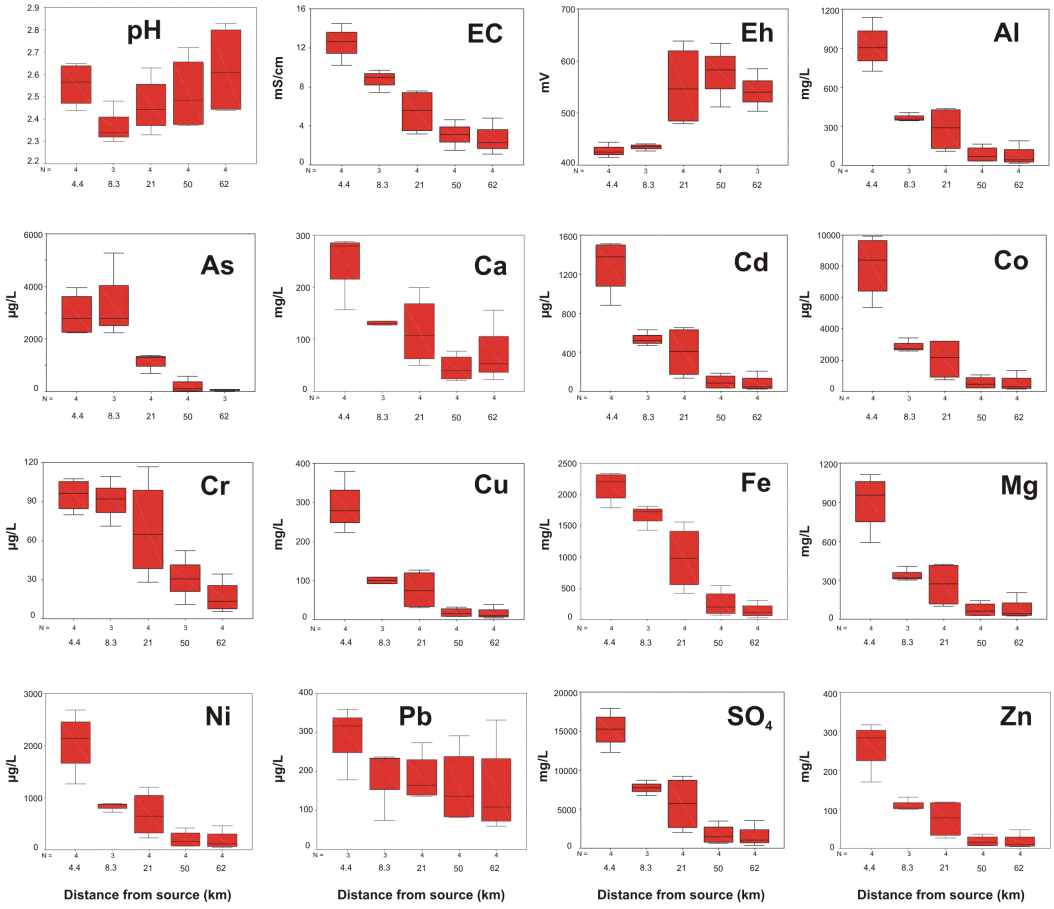

583

584 **Figure 3.** Box-plot and whiskers diagram of main physico-chemical variables, sulphate and
585 metal(loid) concentrations along the Rio Tinto.

586

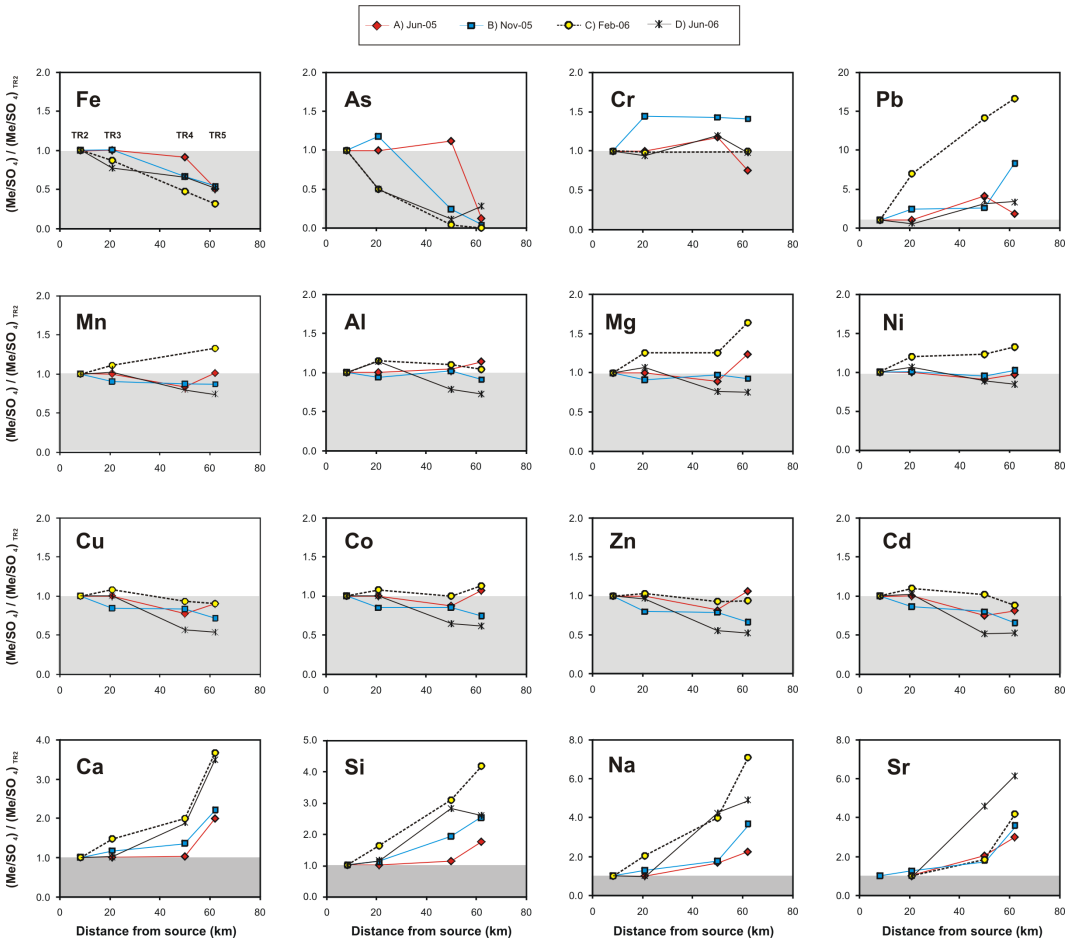

587

588 **Figure 4.** Normalized metal(loid)/sulphate ratios downstream of the mining area.

589

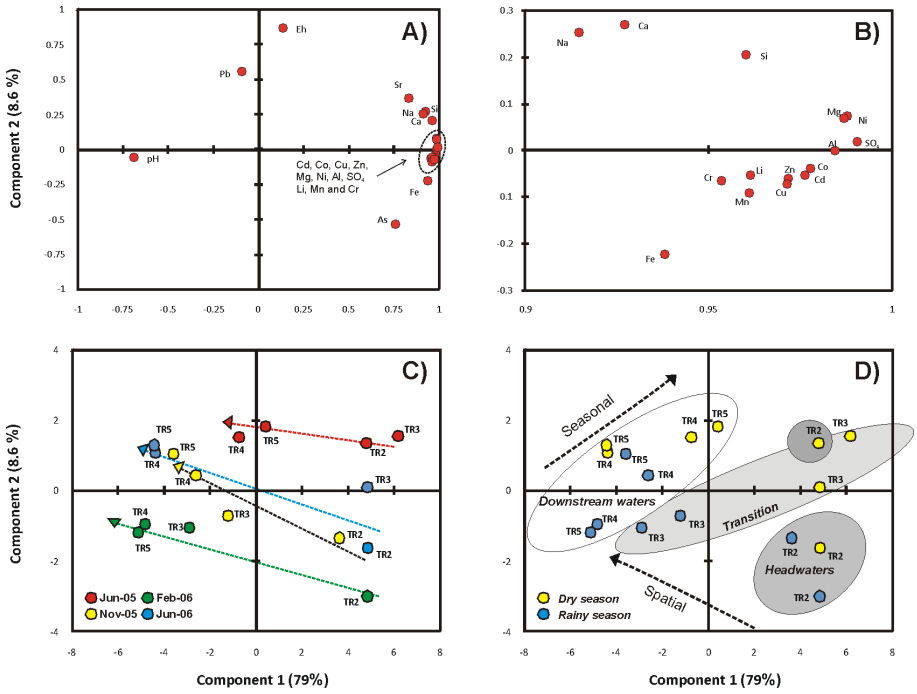

590

591 **Figure 5.** Principal Component Analysis (PCA) performed on the obtained results for variables
592 (A-B) and samples (C-D).

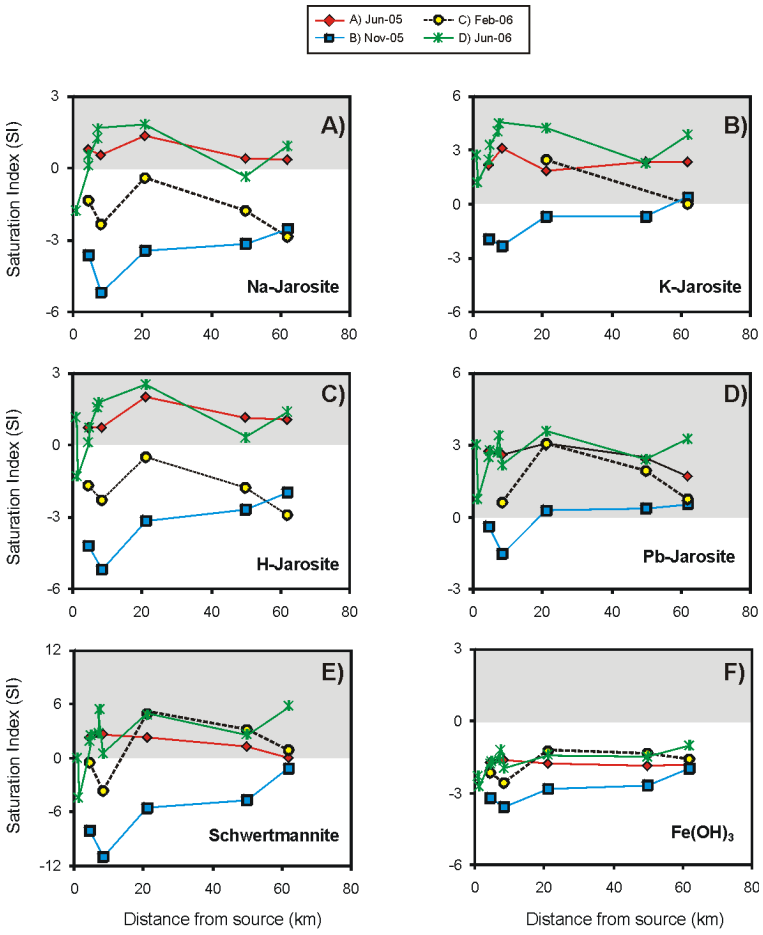

593

594 **Figure 6.** Saturation grade of waters respect some of the main Fe mineral phases precipitating in
595 AMD environments; A-D) jarosite, E) schwertmannite and F) amorphous $Fe(OH)_3$

596

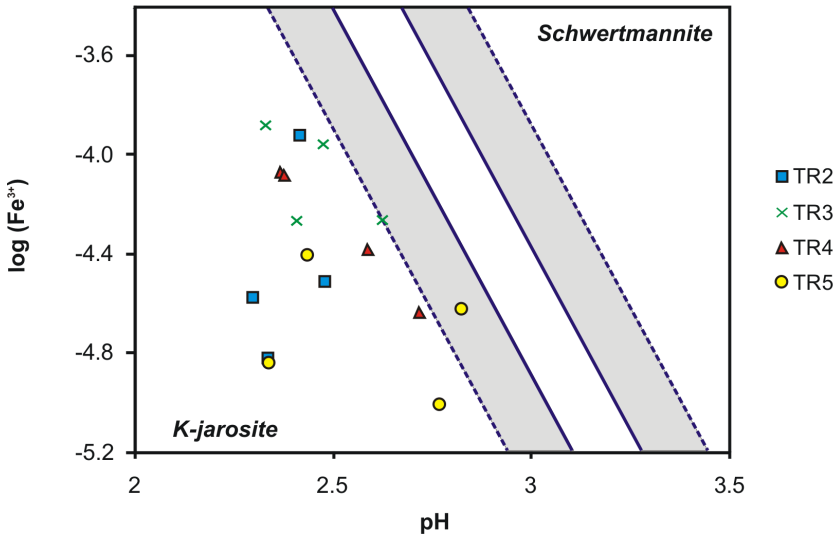

597

598 **Figure 7.** Plot of Fe^{3+} activity against pH in Tinto waters. Solubility windows for schwertmannite
599 (Ks= -18 ± 2.5) and K-jarosite (Ks= -9.21) are constructed from maxima and minima values
600 of K^+ and SO_4^{2-}.

601

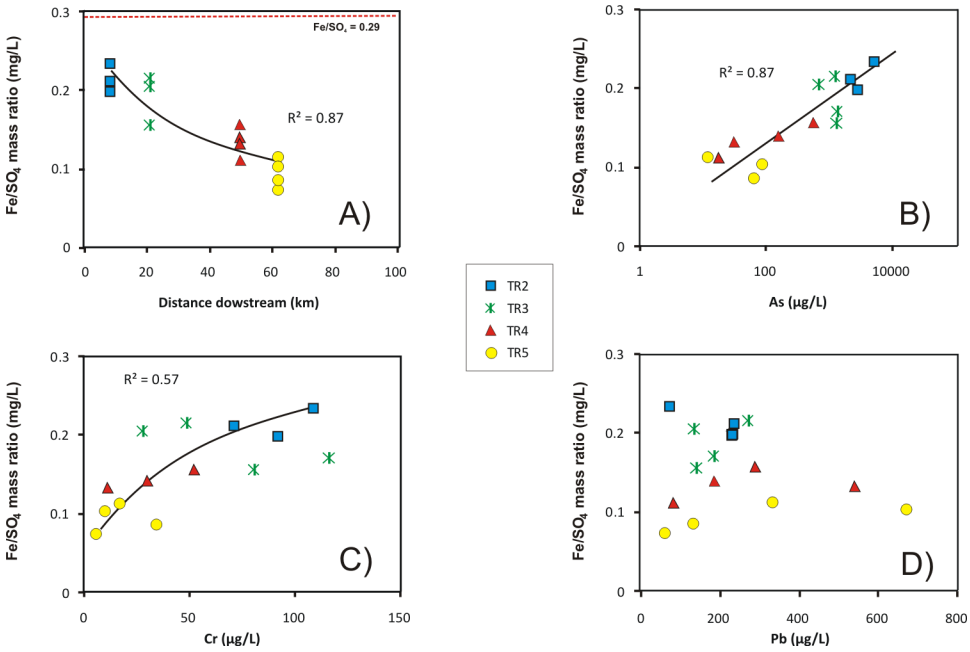

602

603 **Figure 8.** A) Evolution of Fe/SO_4^{2-} along the Rio Tinto; B) Relationship between the Fe/SO_4^{2-}
604 mass ratio and As; C) Cr and D) Pb in Tinto waters.

605

606 **TABLE CAPTIONS**

607

Sample		T1	T2	T3	T4	T5	T6	T7	T8	T9
Locatión		Tinto at Peña del Hierro	Tinto after spoils	Tinto at Nerva	Tinto after Tunnel 11	Tinto before Tunnel 16	Tunnel 16	Tinto after Tunnel 16	Alcojola Creek	Tinto after Alcojola
Distance	km	0,9	1,0	4,4	4,5	7,2	7,3	7,4	8,2	8,3
pH		2,0	2,1	2,7	2,6	2,6	3,0	2,8	1,6	2,5
EC	mS/cm	22	20	15	12	8,9	5,0	7,4	25	9,0
Eh	mV	695	684	628	642	644	612	642	611	636
Al	*Main Elements (mg/L)*	1941	386	1138	881	546	111	381	778	406
Ca		204	147	274	218	172	109	144	252	n.a
Cu		9,9	118	379	274	166	47	119	285	n.a
Fe		10275	1292	2095	1917	1342	735	1115	11574	1723
K		1,6	10	2,7	6,2	12	8,8	11	31	n.a
Mg		1586	403	1114	714	482	301	396	354	405
Mn		86	42	114	78	52	31	43	59	42
Na		38	59	59	56	73	51	64	147	n.a
SO_4		40950	7830	17928	13701	9168	3738	7062	31551	8688
Zn		15	127	317	215	134	90	119	223	131
As	*Trace Elements (µg/L)*	4322	1109	2242	2415	1215	75	792	41951	2786
Ba		11	15	11	13	15	14	19	14	n.a
Be		11	14	54	32	19	5,7	14	14	n.a
Cd		n.a	603	1489	1081	704	393	594	802	630
Co		11628	3384	9931	6328	3948	1856	3202	3894	3417
Cr		142	63	89	83	75	3,2	51	812	92
Li		7182	922	3089	2247	1347	273	912	2871	n.a
Ni		706	861	2216	1663	1073	436	576	1425	885
Pb		418	139	179	184	140	103	134	2052	233
Sn		82	n.a	50	34	42	26	n.a	125	33
Sr		2194	270	428	325	280	277	263	303	n.a

608

609 **Table 1.** Physico-chemical parameters and analytical results of samples collected within the
610 mining area in June 2006.

Sample		TR1				TR2 (T9)				TR3				TR4				TR5			
Location		Tinto at Nerva				Tinto at Zarandas				Tinto at Berrocal				Tinto at Gadea				Tinto at Niebla			
Distance	km	4,4				8,3				21				50				62			
Date		jun.-05	nov.-05	feb.-06	jun.-06	jun.-05	nov.-05	feb.-06	jun.-06	jun.-05	nov.-05	feb.-06	jun.-06	jun.-05	nov.-05	feb.-06	jun.-06	jun.-05	nov.-05	feb.-06	jun.-06
pH		2,6	2,5	2,4	2,7	2,4	2,3	2,3	2,5	2,3	2,4	2,6	2,5	2,4	2,4	2,7	2,6	2,4	2,5	2,8	2,8
CE	mS/cm	13	13	10	15	7,0	7,4	9,7	9,0	7,3	3,8	3,2	7,6	4,6	3,2	1,5	3,1	4,8	2,2	1,1	2,4
Eh	mV	624	630	657	628	610	642	646	636	832	691	700	797	828	795	722	777	775	n.a	713	733
Al	*Main Elements (mg/L)*	883	926	725	1138	375	343	355	406	419	155	108	435	162	105	32	32	187	53	18	32
Ca		287	285	157	274	171	134	128	n.a	200	76	50	138	77	54	21	28	156	50	23	56
Cu		284	273	223	379	101	91	109	n.a	112	37	31	127	33	23	8,4	7,7	39	11	4,8	7,9
Fe		2332	2310	1784	2095	1337	1425	1812	1723	1559	690	416	1265	543	280	71	115	307	130	28	98
K		0,49	0,96	n.a	2,7	1,0	5,3	n.a	n.a	n.a	2,6	2,9	3,3	0,92	1,3	n.a	<3,7	1,4	4,1	1,9	5,9
Mg		1004	906	589	1114	407	317	300	405	422	137	99	407	143	93	31	31	204	50	24	33
Mn		88	124	66	114	35	39	34	42	37	17	10	42	12	10	<2,5	3,4	15	5,7	2,2	3,4
Na		96	162	69	59	62	58	52	n.a	68	36	28	51	43	30	17	23	60	36	18	29
SO_4		15672	14885	12264	17928	8066	6739	7740	8688	9165	3214	2040	8187	3479	2006	636	873	3585	1141	378	948
Si		50	46	38	44	38	27	28	31	48	14	12	34	21	15	7,1	8,8	33	11	5,7	8,8
Zn		279	288	170	317	108	103	100	131	116	39	27	119	36	24	7,6	7,2	48	11	4,6	7,5
As	*Trace Elements (µg/L)*	2255	3289	3943	2242	824	2229	5277	2786	1371	1247	690	1325	582	158	18	32	64	12	n.a	87
Ba		2,7	b.d.l	n.a	11	6	b.d.l	n.a	n.a	29	9,0	12	12	16	9,2	22	89	11	21	28	90
Be		67	66	23	54	20	17	10	n.a	23	6,4	n.a	12	6,5	3,7	n.a	n.a	8,8	b.d.l	n.a	n.a
Cd		1509	1268	883	1489	598	516	466	630	650	212	135	606	186	124	39	33	206	57	20	36
Co		7415	9403	5379	9931	2960	2720	2571	3417	3187	1111	735	3219	1051	691	211	223	1330	342	142	231
Cr		103	107	80	89	99	71	109	92	117	49	28	81	52	30	n.a	11	34	17	5,3	9,8
Li		1364	1432	1773	3089	588	475	832	n.a	632	222	176	1000	268	155	89	134	321	90	60	126
Ni		2687	2063	1262	2216	1067	865	725	885	1204	418	229	883	415	244	73	79	457	149	47	81
Pb		317	359	n.a	179	254	236	74	233	186	273	137	143	292	186	86	82	133	332	60	84
Sn		258	70	18	50	109	14	50	33	98	5,7	49	27	28	b.d.l	37	28	24	n.a	14	22
Sr		563	527	219	428	347	269	152	266	379	168	106	235	297	145	61	115	443	163	82	167

Table 2. Physico-chemical parameters and analytical results of samples collected along the Tinto river course.